DIELECTRIC BREAKDOWN OF CELL MEMBRANES

U. ZIMMERMANN, G. PILWAT, *and* F. RIEMANN

From the Institute of Physical Chemistry of the Nuclear Research Center, Jülich, West Germany

ABSTRACT With human and bovine red blood cells and *Escherichia coli* B, dielectric breakdown of cell membranes could be demonstrated using a Coulter Counter (AEG-Telefunken, Ulm, West Germany) with a hydrodynamic focusing orifice. In making measurements of the size distributions of red blood cells and bacteria versus increasing electric field strength and plotting the pulse heights versus the electric field strength, a sharp bend in the otherwise linear curve is observed due to the dielectric breakdown of the membranes. Solution of Laplace's equation for the electric field generated yields a value of about 1.6 V for the membrane potential at which dielectric breakdown occurs with modal volumes of red blood cells and bacteria. The same value is also calculated for red blood cells by applying the capacitor spring model of Crowley (1973. *Biophys. J.* 13:711). The corresponding electric field strength generated in the membrane at breakdown is of the order of $4 \cdot 10^6$ V/cm and, therefore, comparable with the breakdown voltages for bilayers of most oils. The critical detector voltage for breakdown depends on the volume of the cells. The volume-dependence predicted by Laplace theory with the assumption that the potential generated across the membrane is independent of volume, could be verified experimentally. Due to dielectric breakdown the red blood cells lose hemoglobin completely. This phenomenon was used to study dielectric breakdown of red blood cells in a homogeneous electric field between two flat platinum electrodes. The electric field was applied by discharging a high voltage storage capacitor via a spark gap. The calculated value of the membrane potential generated to produce dielectric breakdown in the homogeneous field is of the same order as found by means of the Coulter Counter. This indicates that mechanical rupture of the red blood cells by the hydrodynamic forces in the orifice of the Coulter Counter could also be excluded as a hemolysing mechanism. The detector voltage (or the electric field strength in the orifice) depends on the membrane composition (or the intrinsic membrane potential) as revealed by measuring the critical voltage in *E. coli* B harvested from the logarithmic and stationary growth phases. The critical detector voltage increased by about 30% for a given volume on reaching the stationary growth phase.

INTRODUCTION

A Coulter Counter is an electric transducer for the counting and sizing of nonconducting particles suspended in an electrolyte medium. The principle of operation of the Coulter Counter is based on the change in electrical resistance that occurs when the suspension is sucked through a narrow orifice across which there exists an electric field. To a first approximation, the resulting current or voltage pulse is proportional

to the size (size = shape factor × volume) of the particle. Therefore, the particle size distribution can be obtained by a pulse height analysis after a linear amplification. Due to the inhomogeneities of the electric field strength in and near to the orifice the pulse height is dependent on the path of the particle through the orifice and on its orientation. Hence, the resulting size distribution is distorted (skewed) (1,2). An extensive analysis concerning the electrical and hydrodynamic factors involved in the transduction of particle size into resistance change in such orifices was given by Grover et al. (3–5). As demonstrated elsewhere (6–9) an unskewed and true representation of a particle size distribution can be obtained by hydrodynamic focusing of the suspension stream. With this improved detector system all particles travel along the same path at the center of the orifice and with the same orientation and therefore, skewness is eliminated.

In measuring the size distribution of particles with this detector system it would be expected that the pulse height corresponding to each size of the distribution would increase linearly with increasing detector current, as predicted by Ohm's law. This is indeed true for Latex particles and fixed cells, but using living bacteria, red blood cells, and algal cells a rather sharp bend in the expected linear curve was observed (6,8,10). Since a conceivable change of the shape factor could be excluded (8) (see also below), the change in slope pointed to an increase of the conductance of the cell membrane which normally acts as an insulator. When the current flows partly through the cell interior the cell volume will be underestimated. This is so because the change in resistance of the current constriction due to the presence of a conducting particle as it passes through the orifice is less than that caused by a nonconducting particle of the same size. The increase of the membrane conductance inferred has been interpreted in terms of a dielectric breakdown, although a "punch-through" effect was also considered. A "punch-through" effect was first observed by Coster (11–13). On measuring the current-voltage characteristics of the membranes of *Chara australis* Coster found for sufficiently large hyperpolarizing potentials that the current suddenly increased very markedly. In contrast to dielectric breakdown "punch-through" results in a reversible permeability change of the membrane, i.e. without "rupture" of the membrane. As described elsewhere (8,10), we could demonstrate that for red blood cells a total release of hemoglobin occurred after passage of the cells through the electric field in the orifice. Hence, it may be safely assumed that the observed shift in the size distribution towards smaller values at high detector currents does not reflect a "punch-through" effect.

In this paper, we bring together all the data of experiments which support the notion of the dielectric breakdown phenomenon and virtually rule out the alternative mechanism of mechanical rupture of the membrane which could perhaps contribute partly to the apparent breakdown, particularly when using red blood cells or algal cells lacking a cell wall (8). These latter cells are deformed strongly by the hydrodynamic forces in the orifice (9). Finally we tried to elucidate some parameters on which the critical detector current, producing breakdown, depends.

MATERIALS

Human and bovine blood was withdrawn from apparently healthy donors and stored under sterile conditions in ACD buffer at 4°C for not more than 2 days. The red blood cells were prepared in the usual way (14). For sizing at different detector currents the cells were suspended in isotonic NaCl-solution (0.9%).

E. coli B 163, requiring methionine, histidine, and leucine for growth, were grown and harvested as described in detail previously (15). Breakdown investigations were performed for cells harvested from the logarithmic as well as from the stationary growth phase in the same electrolyte, i.e., in the nutritive medium of the following composition: KCl, 30 mM; $MgCl_2$, 1 mM; Na_2HPO_4, 90 mM; NaH_2PO_4, 30 mM; $(NH_4)_2SO_4$, 15 mM; glucose, 0.5%, histidine and leucine 100 mg/l.

Methionine was omitted so as to stop the growth during the measurement period.

METHODS

Coulter Counter

Electronic measurement of size was performed with a Coulter Counter (AEG-Telefunken, Germany). The detector system and the hydrodynamic focusing of the suspension stream were described previously (6). For measuring bacteria suspensions an orifice 20 μm, in diameter and length, was used; for measuring red blood cells an orifice 40 μm, in diameter and length, was

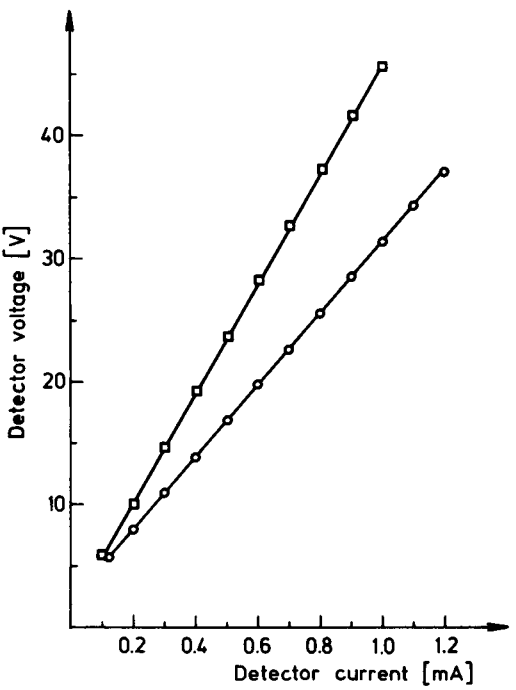

FIGURE 1 Current-voltage characteristic for a detector orifice of a diameter of 20 μm (squares), electrolyte: nutritive medium; and of 40 μm (circles), electrolyte: 0.9% NaCl solution.

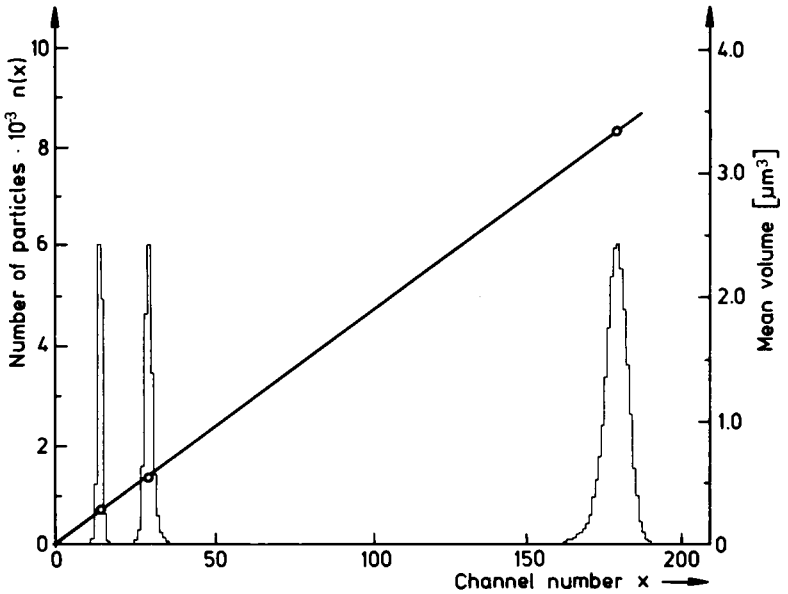

FIGURE 2 Size distribution of Latex particles with diameters of 0.810 μm, 1.011 μm, and 1.857 μm. Orifice: 20 μm in diameter and length; detector current: 1.0 mA; electrolyte: 0.9% NaCl solution. Plots of the mean volume (given by the manufacturer) of the particles (right ordinate) vs. the pulse height of the mean (modal) size, showing the linear relationship between these parameters.

used. The velocity of the flow through the orifice was about 2 m/s. The electronic parameters for the amplification of the pulses generated by the passage of the particles through the orifice were set according to the manufacturers instructions. A crucial condition for the investigation of dielectric breakdown phenomena by means of this Coulter Counter is the requirement that the voltage-current-characteristic of the detector system be linear and that a pulse height be linearly dependent on the size of the particles at given conductivities of the electrolyte, detector currents, and amplifications. Fig. 1 shows the voltage current characteristic of the 20-μm and 40-μm orifices. It is seen that a linear dependence exists for detector currents in the range of 0.1–1.2 mA. Fig. 2 shows the mean volume of Latex particles, of different diameters, measured with an orifice of 20 μm, as a function of the channel number (pulse height) corresponding to the mean (= modal) size. The correlation coefficient for the straight line is 0.9999, indicating that the pulse height indeed does depend linearly on volume. The same result was obtained with an orifice 40 μm in diameter and length.

Impulse Method

In order to rule out mechanical rupture of red blood cells by deformation in the hydrodynamic flow field in the orifice, dielectric breakdown was also investigated by placing red blood cell suspensions between two flat platinum electrodes (2.5 × 2.5 cm) in a thermostated Plexiglas chamber. The distance between the electrodes was 1 cm, and the chamber was a part of a high-voltage discharge circuit (16). The high voltage storage capacitor was discharged via a spark gap and in this way the potentials were applied to the electrodes of the chamber. The voltages were varied between 2 and 7 kV. The resistance of the chamber when filled with the suspension was 10 Ω and the electrical decay constant was 27 μs. After application of the potential the

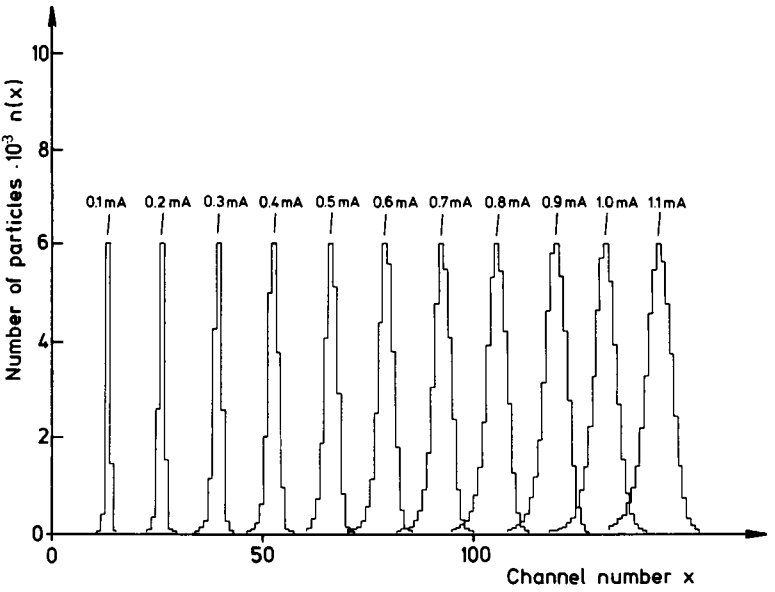

FIGURE 3 Size distributions of Latex particles (1.857 μm in diameter) as a function of detector current (0.1–1.1 mA). Orifice: 20 μm in diameter and length; electrolyte: 0.9% NaCl solution.

suspensions were centrifuged at 10,000 *g*, and the hemoglobin released in aliquots of supernate were measured with a Zeiss spectrophotometer (Carl Zeiss, Inc., New York) at 398 nm.

RESULTS AND DISCUSSION

Size Distributions and Their Dependence on the Detector Voltage

In Fig. 3 the size distributions of Latex particles (diameter = 1.857 μm) measured with a 20 μm orifice are given at different detector currents (0.1–1.1 mA). The size distributions are normally distributed. The standard deviation is of the same order as the deviation given by the manufacturer (Serva, Germany) (see also ref. 9). For reasons of clarity plots are also given in Fig. 4 of the dependence of the pulse heights (channel numbers) of the size distributions on the detector voltage. The voltage values were calculated from the voltage current characteristic of a 20 μm orifice as shown in Fig. 1. For each size a linear curve is obtained with a correlation coefficient of 0.9999.

In Fig. 5 typical size distributions of human red blood cells at different detector currents are plotted. The size distributions are normally distributed. Similar size distributions were also found for bovine red blood cells (10). Calibration of the channel numbers with Latex particles size distribution the mean (= mode) volume of the human and bovine red blood cells could be calculated from

$$V_R = (f_L/f_R)V_L, \tag{1}$$

where f_L and f_R are the shape factors of the Latex particles and of the red blood

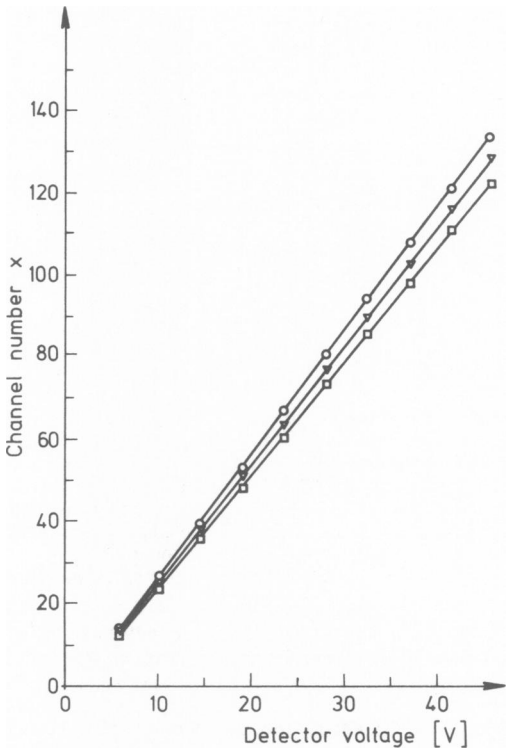

FIGURE 4 Pulse heights (channel numbers) of the size distributions presented in Fig. 3 as a function of the detector voltage. The detector voltage was calculated from the current-voltage characteristic of Fig. 1. Triangles: pulse heights corresponding to the modal (= mean) volume of 3.353 μm^3; squares: pulse heights corresponding to a smaller volume of 3.194 μm^3; circles: pulse heights corresponding to a larger volume of 3.497 μm^3.

cells, respectively, and V_L the volume of the Latex particles. The shape factor of the spherical Latex particles was 1.5, whereas the shape factor of the human and bovine red blood cells was 1.07 according to Thom (9). The shape factor for the red blood cells is smaller than the value of 1.18 measured by Grover et al. for the α-mode of human red blood cells, largely because of the large hydrodynamic forces at the entrance of the orifice in our detector system. Using the above values for the shape factors, the average mean volume of human and bovine red blood cells was calculated to be 81 μm^3 (76–87 μm^3, in 7 measurements) and 51 μm^3 (43–57 μm^3, in 11 measurements), which is in agreement with literature (9).

On plotting different pulse heights (channel numbers) of the human and bovine red blood cell size distributions against detector voltage characteristic sharp bends in the linear curves were observed (Fig. 6 *a* and 6 *b*). The correlation coefficients are 0.9998 for all curves below and above the critical voltage at which the change in slope occurs. The critical voltage depends on the cell size, i.e. with increasing size the critical voltage

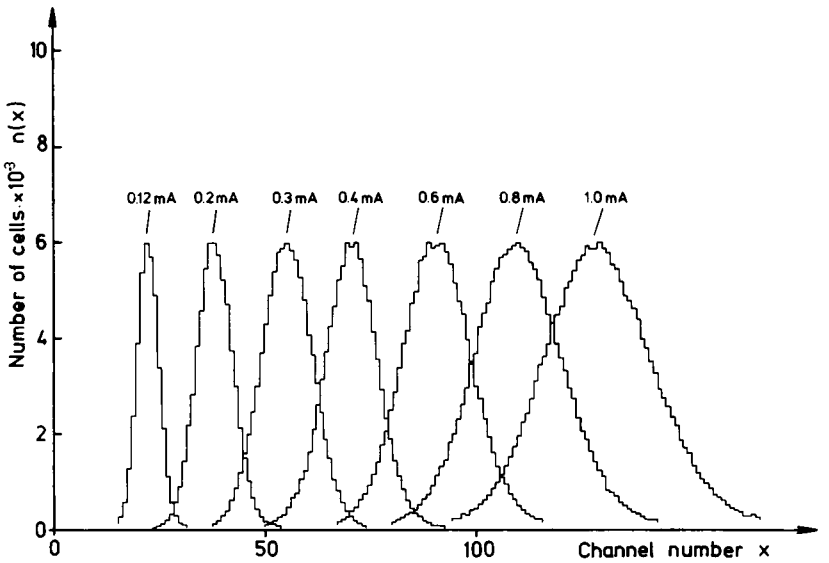

FIGURE 5 Size distributions of human red blood cells as a function of the detector current (0.12–1.0 mA). Orifice: 40 μm in diameter and length; electrolyte: 0.9% NaCl solution.

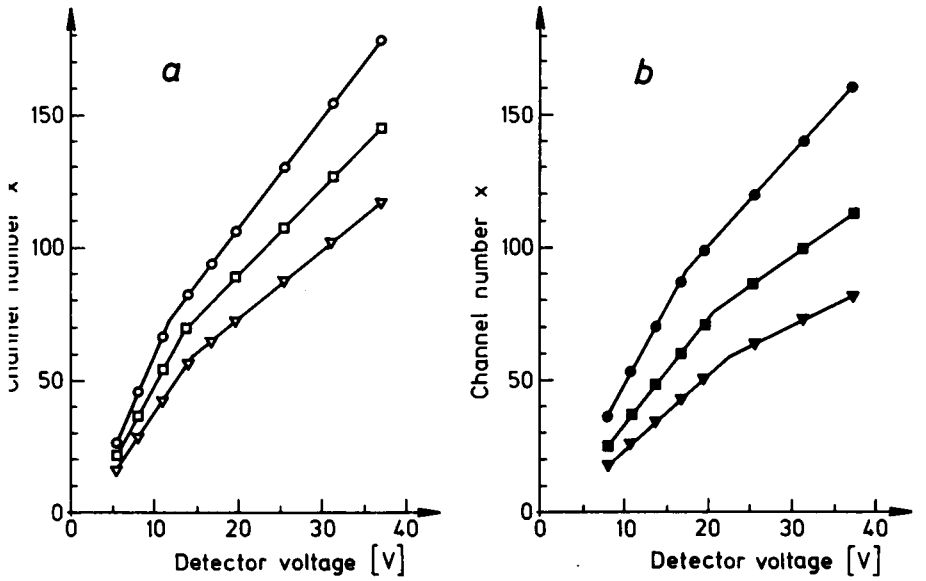

FIGURE 6 Dielectric breakdown of the membrane of human and bovine red blood cells. Pulse heights (channel numbers) of the size distributions of human red blood cells (presented in Fig. 5), and bovine red blood cells (not shown) are plotted as a function of the detector voltage. The detector voltage was calculated from the current-voltage characteristic of Fig. 1. (Part *a*: human red blood cells; part *b*: bovine red blood cells). Squares: pulse heights corresponding to the modal (= mean) volume of 80.7 μm^3; triangles: pulse heights corresponding to a smaller volume of 62.9 μm^3; circles: pulse heights corresponding to a larger volume of 100.3 μm^3. Filled squares: pulse heights corresponding to the modal (= mean) volume of 48.9 μm^3; filled triangles: pulse heights corresponding to a smaller volume of 36.5 μm^3; filled circles: pulse heights corresponding to a larger volume of 74.0 μm^3. The volumes were calculated from Eq. 1.

decreases. Since bovine red blood cells are smaller, the critical voltages are always higher than those required for the same sizes of human red blood cells.

The apparent shift of the human and bovine red blood cell size distributions towards smaller values at higher detector currents or voltages could at first sight perhaps be thought to arise from a change of the shape factor, particularly on taking into account the theoretical calculations of Allan and Mason (17) and experimental results obtained by Grover et al. (5) on the influence of the electric field strength on shape. Grover et al. observed that at a certain critical electric field strength in the orifice the size (but not the volume!) of the cells decreased for an increase in field strength. The value of the critical electric field strength above which the apparent size was changed, was about 0.8 kV/cm for human red blood cells in isotonic phosphate-buffered saline and was independent of the orifice dimension and the current. This value is much lower than the critical voltages observed in our experiments (see also below). Furthermore, a change in the shape factor value cannot play a large role in our detector system, since for example the mean size of the human red blood cell size distributions is underestimated by 33%. This would correspond to a change in the shape factor from 1.0 to 0.75, which is impossible since the lowest limit of the shape factor is 1.0 for an infinite cylindrical particle.

Therefore, the sharp bend must be related to a change of the effective volume measured by the Coulter Counter. This is particularly indicated by our previous measurements on bacteria (6), where no deformation was observed due to the rigid cell wall. The only adequate explanation then is that the conductance of the membranes increases at a certain critical voltage or electric field strength in the orifice.

Calculation of the Critical Membrane Potential

The potential, V_M, generated across the membrane which was responsible for the change in the membrane conductance, can be roughly calculated by the application of the Laplace theory (Appendices I and II). Assuming a linear potential gradient E_0 in

TABLE I

V_M CALCULATED FOR BOVINE AND HUMAN RED BLOOD CELLS IN THE 40 μm ORIFICE OF THE COULTER COUNTER

	Modal volume	Radius*	Major semi-axis‡	Minor semi-axis‡	Breakdown§ detector voltage	External field strength E_0	V_M, spherical coord.	V_M, ‖ ellipsoidal coord.
	μm^3	μm	μm	μm	V	$V \cdot cm^{-1}$	V	V
Human red blood cells	80	2.67	6.34	1.74	13	3,250	1.3	2.2
Bovine red blood cells	45	2.21	5.25	1.44	16.8	4,200	1.4	2.3

*Radius of the corresponding spherical volumes.

‡Data calculated for prolate ellipsoids according to Thom (9).

§Data taken from Fig. 6.

‖ Calculated from the major semi-axis parallel to the external field strength.

TABLE II

V_M CALCULATED FOR *E. COLI* B 163 IN THE 20 μm ORIFICE OF THE COULTER COUNTER

	Cell volume	Radius*	Major semi-axis‡	Minor semi-axis‡	Breakdown§ detector voltage	External field strength E_0	V_M, spherical coord.	V_M, ellipsoidal coord.
	μm^3	μm	μm	μm	V	$V \cdot cm^{-1}$	V	V
E. coli B163	1.43	0.702	1.425	0.49	20.4	10,200	1.1	1.6

*Radius of the corresponding spherical volume.

‡Data taken from electron micrographs.

§Data taken from Fig. 9 for the logarithmic phase of growth.

‖Calculated for the major semi-axis parallel to the external field.

the orifice the membrane potential V_M generated for spherical particles is given by Eqs. 15 and 16, and for ellipsoidal particles by Eq. 17. Using 4.2 kV/cm for the linear gradient calculated from Fig. 6 *b*, V_M is calculated to be 1.4 V for the modal volume of 45 μm^3 of the bovine red blood cell distribution (using a spherical approximation) and about 2.3 V (using an ellipsoidal approximation) (Table I). Values of the same order of V_M were also obtained for the mode volumes of human red blood cells (1.3 resp. 2.2 V) and bacteria (1.1 resp. 1.6 V) (Table II). If we assume that the critical membrane potential V_M is independent of the volume, the critical external electric field strength (or the detector voltage and current, respectively) should increase for decreasing cell volume (Eqs. 15–17).

This was found experimentally for bacteria and red blood cells. In Fig. 7 the dependence of the external electric field strength is plotted versus the volume of the bovine red blood cells. The data for these plots were taken from Fig. 6 *b*. Bovine red blood cells were used since the distributions are broader than those of human red blood cells and bacteria. If we use an average value of 1.6 V for V_M the dependence of the external electric field strength on volume can be calculated from Eq. 15. According to Fig. 7 the agreement between the theoretical calculation and the experimental finding is fairly good.

If we assume that the voltage of 1.6 V drops across the bimolecular lipid leaflet the electric field strength in the membrane is on the order of 4 to $5 \cdot 10^6$ V/cm. This value is comparable with the breakdown voltages for bilayers of most oils which are on the order of $20 \cdot 10^6$ V/cm (18), particularly if the intrinsic membrane electric field strength is taken into account on which the applied electric field strength is superimposed. The magnitude of the intrinsic electric field can be estimated assuming that the double fixed charge model used by Coster (13) to explain the "punch-through" effect is also an adequate model for dielectric breakdown.

Coster's calculations are based on the proposition that the trilayer structure of the cell membranes seen under the microscope reflect a double fixed charge model rather than a dimensionally fixed bimolecular layer. In the model one-half of the membrane

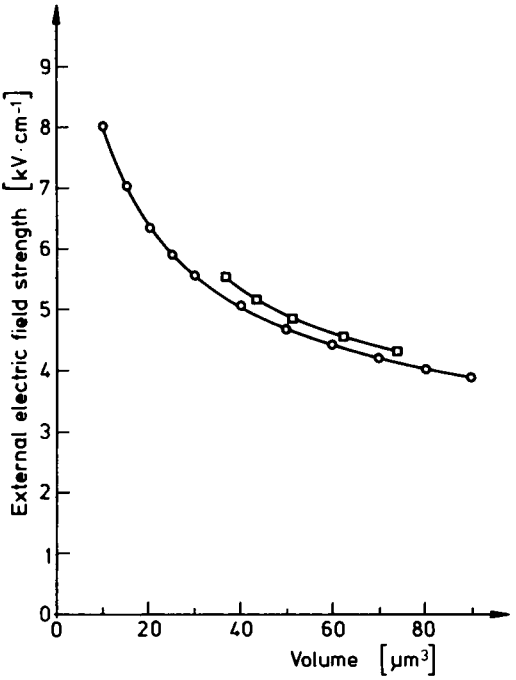

FIGURE 7 The external electric field strength producing dielectric breakdown as a function of the particle volume. Circles: external electric field strength (calculated from Eq. 15) vs. the volume; squares: external field strength as a function of the cell volume. The field was calculated from the critical detector voltage of bovine red blood cell distributions measured with an orifice of a diameter and length of 40 μm. Data were taken from Fig. 6 *b*.

contains a predominance of positive charges and the other a predominance of negative charges. The junction between the two lattices bearing charges of opposite signs gives rise to a transition region, the depletion layer, in which the space charge density is very high due to the lack of mobile counterions. Therefore, the electric field strength in this central region is very high compared with the weak electric field strength in the remainder of the two lattices. Coster calculated a value of the order of 10^6 V/cm for the electric field strength in the depletion layer, even with zero potential across the membrane. This means that the intrinsic electric field strength could contribute considerably to the total electric field strength, which is responsible for the discontinuity observed.

It is also necessary to consider a possible contribution of a polarization mechanism involving the ionic atmosphere on the cell surface as discussed by Neumann and Rosenheck (16) for chromaffin granules. In general, the surface charge density of the membrane is very high. Therefore, the ion density in the ion cloud is much higher than that of the surrounding electrolyte. A displacement of the ion cloud relative to the surface due to the electric field in the orifice results in a polarization. The relaxation time τ of the counterion polarization can be calculated according to Schwarz (19) from

(for spherical particles),

$$\tau = r^2/2ukT, \tag{2}$$

where r is the radius, u the mobility of the counterions in the ionic atmosphere, T the absolute temperature, and k the Boltzmann constant. Using a mean value of 2 μm for the radius of bovine red blood cell, a value of $6 \cdot 10^8$ cm $\cdot$ s^{-1} $\cdot$ dyn^{-1} for the mobility u, and T = 295°K, the relaxation time is calculated to be 820 μs. For bacteria (see below) the relaxation time is about 75 μs, using a mean radius of about 0.6 μm. Since the particles cross the orifice in 20 μs as found by pulse observation with an oscilloscope we can conclude that a polarization effect cannot play an important role in our experiment.

The calculated voltages and the agreement between the theoretical and experimental volume dependence of the critical voltages point to a dielectric breakdown of the cell membranes in the orifice of the Coulter Counter. This assumption is also supported by applying the electromechanical model of Crowley (18) to our results. Crowley investigated the electrical breakdown of bimolecular lipid membranes and considered the membrane as an elastic system subject to a compressive electric force caused by applied voltages. The treatment of the bilayer film in this way was supported by the work of White and Thompson (20). Crowley calculated the stability of an elastic condensator (capacitor spring model) assuming that the elastic force which obeys Hooke's law between the capacitor plates, is balanced by the electric compressive tension.

$$-\epsilon V^2/2l^2 = \mathrm{E} \cdot \ln (l/L) \tag{3}$$

where E is Young's modulus, ϵ is electrical permittivity, l is thickness of the membrane at voltage V, and L is original thickness of the membrane.

Introducing $\Delta = L - l$ and expanding the logarithmic function in Eq. 3 in a Taylor series, the relative change of the distance between the two plates (the thickness) is initially proportional to the square of the voltage,

$$\Delta/L \simeq \epsilon V^2/2EL^2 = (C_0 \cdot V^2)/2EL \tag{4}$$

where $C_0 = \epsilon/L$ is the capacitance. A numerical solution of Eq. 3 shows that the displacement approaches infinity for a finite value of V and that such an electromechanical instability occurs at a value of 0.18 for $\epsilon V^2/2EL^2$.

Crowley could also show that the same equation for the critical voltage producing breakdown is obtained using a flexible membrane model. Using an average of $7 \cdot 10^7$ dyn/cm^2 (21,22) for the Young's modulus of the human red blood cells (but see also the objections against this value made by Hochmuth et al. [23]) and for $C_0 = 1$ μF (24), the critical voltage producing breakdown was calculated to 1.6 V. This value is in very good agreement with our present results calculated with the use of Laplace's theory, without consideration of the intrinsic potentials in the membrane. We feel that this is not a fortuitous result, but further confirms our dielectric breakdown hypothesis.

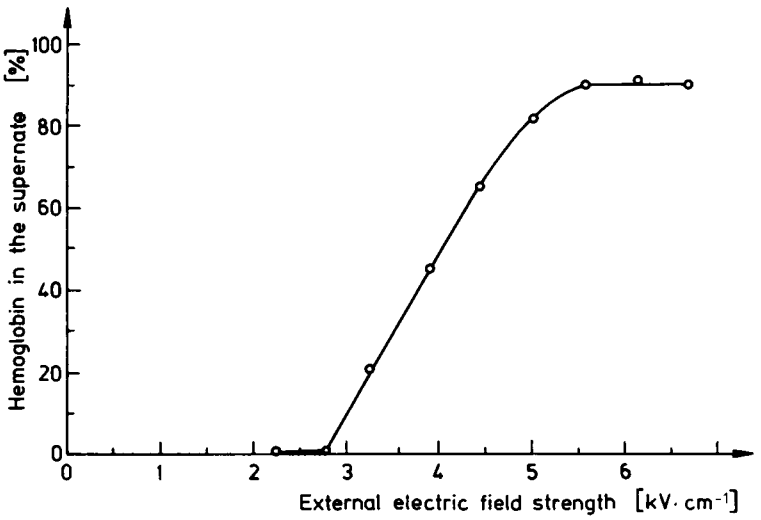

FIGURE 8 Dielectric breakdown of bovine red blood cells in homogeneous electric fields. The content of hemoglobin in the supernate as a function of the total hemoglobin content is here plotted as a function of the applied field strength.

Dielectric Breakdown in Homogeneous Electric Fields

Since the electric field in the orifice is nonuniform and the assumption of a linear gradient for the solution of the Laplace equation is very rough, we performed experiments on the effect of an electric field on red blood cells suspensions between two flat, platinum electrodes in a thermostated Plexiglas chamber. The electric field was applied by discharging a high voltage storage capacitor via a spark gap. Bovine red blood cells were used since it was discovered recently that a total release of hemoglobin from red blood cells occurs after passage through the orifice of the Coulter Counter if the detector current was high enough. As pointed out earlier this finding eliminates other possible mechanisms such as a "punch-through" effect or a transient membrane permeability change (as detected by Neumann and Rosenheck in the membranes of vesicles storing biogenic amines [16]—see also above).

This experiment was also performed to show whether or not mechanical breakdown (21, 25) as well as the electrical breakdown phenomenon needs to be taken into account. The results of these experiments are shown in Fig. 8. The hemoglobin content of the supernate, which was taken as indicator of cells in which dielectric breakdown had occurred, is here plotted against the external electric field strength. A nearly S-shaped curve is obtained. The start of dielectric breakdown is observed at 2.7 kV/cm. At 5.5 kV/cm nearly all cells had lost their hemoglobin. The inflection point of the curve indicates the dielectric breakdown of the mean (or mode) of the size distribution. The external field strength of 4.4 kV/cm corresponds quite closely to the 4.2 kV/cm obtained for the breakdown field strength in the orifice of the Coulter Counter.

However, the electric field strengths cannot be compared directly since the shape

TABLE III

V_M CALCULATED FOR BOVINE RED BLOOD CELLS IN THE HOMOGENEOUS FIELD (PLEXIGLAS CHAMBER)

	Modal volume	Radius*	Major semi-axis‡	Minor semi-axis‡	External field strength E_0	V_M, spherical coord.	V_M,§ ellipsoidal coord.	V_M,‖ ellipsoidal coord.
	μm^3	μm	μm	μm	$V \cdot cm^{-1}$	V	V	V
Bovine red blood cells	45	2.21	3.1	1.8	4,400	1.4	1.6	1.4

*Radius of the corresponding spherical volume.
‡Modified data according to Thom (9).
§Major semi-axis parallel to the external electric field.
‖ Minor semi-axis parallel to the external electric field.

and the orientation of the cells in the electric field were different in the two experiments. In the orifice of the Coulter Counter the oblate red blood cells were deformed to prolate ellipsoids and were orientated with their major semi-axis parallel to the electric field as mentioned above. In contrast, between the two electrodes in the Plexiglas chamber the oblate red blood cells were randomly orientated relative to the direction of the electric field.

As shown in Table III the average value for the membrane potential, V_M generated in the homogeneous field, calculated from Eq. 16, is about 1.45 V. This is the mean value of the potentials generated for oblate cells oriented with their major semi-axis parallel and perpendicular to the electric field. This value is of the same order as was found for prolate deformed cells in the orifice. Thus we can exclude a mechanical rupture of the membrane as an explanation of our findings. This is also supported by the finding that red blood cells sucked through the orifice without applying a voltage (10) did not lose hemoglobin.

A thermal effect as a possible hemolysing mechanism was also considered by measuring the temperature increase in the Plexiglas chamber and behind the orifice of the Coulter Counter using a thermocouple. The temperature increase was about 3–5°C. This small increase cannot cause the observed effects as proved by Sale and Hamilton (26,27) describing phenomenologically similar effects of high electric fields on numerous microorganisms.

The Dependence of the Dielectric Breakdown Voltage on Membrane Properties

The Crowley model for the breakdown voltage suggests that the critical voltage depends on the composition of the membrane, particularly on that of the bimolecular lipid leaflet. Crowley could demonstrate that the critical voltage for cholesterol is approximately three times that of phosphatidylcholine bimolecular leaflet and that this difference results from different Young's moduli and capacitances. In the following we examined, therefore, how far the critical voltage depends on membrane properties using bacteria (*E. coli* B 163). Red blood cells were not used since preliminary

measurements with different antibiotics and inhibitors indicated that in many cases it was very difficult at this stage to distinguish between changes of the critical voltage caused by a change of the shape factor and those caused by altered membrane properties. These difficulties do not occur with *E. coli* B since no deformation by the hydrodynamic forces in the orifice under different experimental conditions were observed.

The critical membrane potential difference V_M, in bacteria is about 1.1 V (spherical coordinates) and 1.6 V (ellipsoidal coordinates) (Table II). The values agree very well with the values calculated for human and bovine red blood cells (Table I and III).

In order to get a preliminary insight into the dependence of the critical voltage on membrane properties we examined bacteria harvested from the logarithmic and stationary growth phase. Since the relation between the detector current and voltage depends on the conductivity of the electrolyte, the measurements had to be performed in the same solution. Since Eqs. 6 and 17 are valid the influence of the internal conductivity of the cells could be neglected. The size distributions of *E. coli* is positively skewed as was shown previously (6) and as would be expected during the growth stage (28). The shape factor f was calculated from electron micrographs on the assumption that the shape was a composite of a long cylinder with two hemispheres, one on each end. From the evaluation of the spherical part of the total volume with the shape factor of 1.5 and of the cylindrical part with a shape factor of 1.0 the shape factor is given by

$$f = l/(l - 0.33d), \tag{5}$$

where l is length of the particles (bacteria in this case) and d is diameter of the particles.

The shape factor for cells harvested from both the logarithmic and stationary growth phase was 1.13. Since the shape factors were identical we can confine the consideration to the sizes in what follows. Fig. 9 shows the modal size as a function of growth time. The value was constant during the logarithmic phase and drops by 10–15% upon reaching the stationary phase. In order to evaluate changes in the critical voltages for cells harvested from the logarithmic and stationary phase of growth, identical cell sizes of all size distributions must be compared.

The critical detector voltage as a function of the growth time was obtained by measurements of the size distributions according to Fig. 5 and subsequent plotting of the data according to Fig. 6. The correlation coefficients of the linear curves below and above of the critical voltages are 0.9998. According to Fig. 9 the voltage at which dielectric breakdown occurred for a certain size was also constant during the logarithmic phase. This result indicates that the properties of the membranes were uniform during the logarithmic phase of growth. However, after reaching the stationary phase the detector voltage required for dielectric breakdown increased markedly for the same size (by about 30%). From the foregoing discussion we must conclude that this increase was related to a change in membrane composition and/or to a change in intrin-

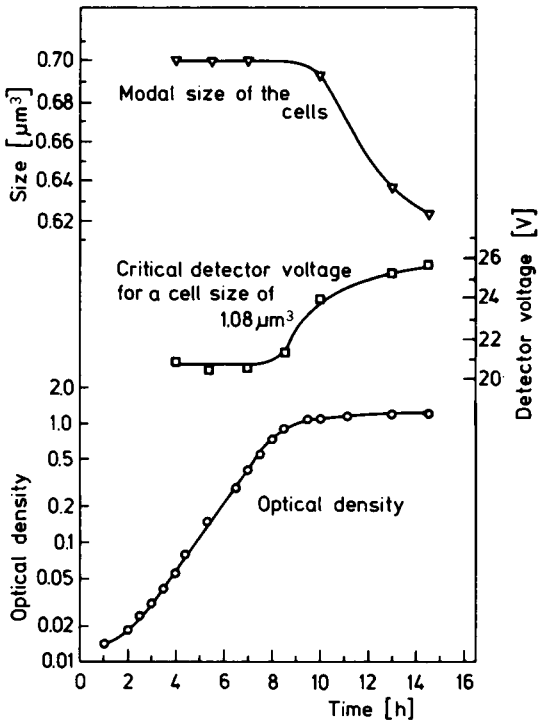

FIGURE 9 Dielectric breakdown of the membrane of *E. coli* B 163 in the logarithmic and stationary phase of growth. The critical detector voltage for a cell size of 1.08 μm^3 is plotted vs. the growth time. For comparison the modal cell size as a function of the growth time is also shown. The optical density is plotted to indicate the growth.

sic membrane potentials (see above). In order to obtain insight into the molecular changes in membrane properties which occur in the stationary phase a correlation between dielectric breakdown, membrane composition and intrinsic membrane potential is required. This data is presently lacking. A useful way to study this phenomenon would be to measure the dependence of dielectric breakdown on membrane potential and to utilize bacterial mutants having a defect in the lipid syntheses (29). The question that remains unanswered is the molecular basis of the dielectric breakdown of the cell membrane. We feel that the model of Crowley and of White (30) which was presented very qualitatively in a short communication relating to the paper of Crowley, could perhaps yield some answers in the near future.

APPENDIX I

In order to calculate the potential drop in the orifice we use the following simplified model for the Coulter Counter. In this two cylindrical containers of the same cross-sectional area are con-

nected by a cylindrical orifice, as shown in the diagram below:

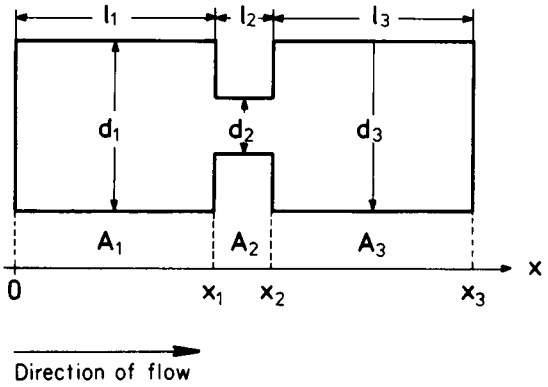

Here l_i = lengths of the cylindrical containers and the orifice, respectively; A_i = cross-sectional areas; and d_i = diameters. The total potential difference V between the two electrodes is given by:

$$|V| = \int_0^{x_3} E(x)dx = \int_0^{x_1} E(x)dx + \int_{x_1}^{x_2} E(x)dx + \int_{x_2}^{x_3} E(x)dx, \quad (6)$$

where E is the electric field strength. The current I and the current density j in the two containers and in the orifice are given by (31–33):

$$I = \int_{A_1} j\,da = \int_{A_2} j\,da = \int_{A_3} j\,da, \quad (7)$$

$$j = \sigma E \quad (8)$$

where σ = electrical conductance.

Combining Eqs. 7 and 8 and on integration, we obtain:

$$I = \sigma E_1 \pi (d_1/2)^2 = \sigma E_2 \pi (d_2/2)^2 = \sigma E_3 \pi (d_3/2)^2, \quad (9)$$

or

$$k = E_1 d_1^2 = E_2 d_2^2 = E_3 d_3^2, \quad (10)$$

where k is a constant. Substituting E in Eq. 6 by Eq. 10 we obtain on integration with $d_1 = d_3$:

$$|V| = (k/d_1^2)(l_1 + l_3) + (k/d_2^2) l_2 \quad (11)$$

or

$$K = ([l_1 + l_3]/d_1^2) + (l_2/d_2^2), \quad (12)$$

where K is a constant.

Using Eq. 12 and the following values appropriate to the Coulter Counter:

$$l_1 + l_3 = 35 \text{ mm} \qquad d_1 = 5 \text{ mm}$$
$$l_2 = 0.02 \text{ mm} \qquad d_2 = 0.02 \text{ mm},$$

we calculate that more than 97% of the total potential difference appears across the orifice.

APPENDIX II

In principle, the potential difference superimposed on the intrinsic membrane potential upon the application of the electric field can be calculated by the solution of the Laplace equation. An analytical solution, however, of the Laplace equation is not possible since the boundary conditions cannot be completely specified. To proceed, therefore, the following simplifying assumptions were made. To a good approximation, the pulse shape due to a particle passing the orifice is like the bell-shaped Gaussian distribution (9). Thus we assume that the potential gradient along the axis of the orifice has the same shape. For a rough calculation of the membrane potential generated we replace the maximum value of the gradient in the center of the orifice by the value of a "linear" potential gradient E_0 (the results obtained for dielectric breakdown in a homogeneous field [see above] justified this approximation). The linear gradient is obtained from the assumption that 97% of the potential difference between the two electrodes drops linearly over the length of the orifice. Furthermore, we postulate that in the center of the orifice a small region exists where the potential drop is nearly homogeneous. Applying the Laplace equation to this region, the equation can be solved in spherical (r, ϑ, φ) and ellipsoidal (ξ_1, ξ_2, ξ_3) coordinates in the usual manner (31–41).

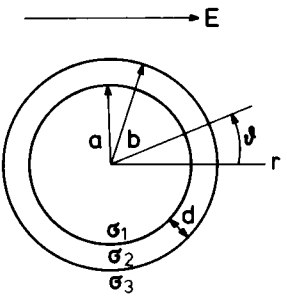

A spherical cell volume is considered having the inner and outer radii a and b, respectively, and a membrane thickness d. σ_1, σ_2, and σ_3 denote the conductivities of the cell interior, the membrane, and the external medium; ϕ_1, ϕ_2, and ϕ_3 denote the potentials in the three regions.

With the boundary condition

$$\phi \rightarrow - E_0 r \cos \vartheta \qquad \text{for } r \rightarrow \infty, \tag{13}$$

with the boundary condition ϕ must be finite for $r = 0$, and the boundary conditions for the interfaces at $r = a$ and $r = b$ yield,

$$\begin{aligned} \phi_1(a) &= \phi_2(a) \\ \phi_2(b) &= \phi_3(b) \\ (\sigma_1/a)(d\phi_1/dr) &= (\sigma_2/a)(d\phi_2/dr) \\ (\sigma_2/b)(d\phi_2/dr) &= (\sigma_3/b)(d\phi_3/dr). \end{aligned} \tag{14}$$

The problem is now well defined and yields the following expression for the potential difference V_M across the membrane,

$$V_M = \frac{\frac{3}{2+\beta} E_0 \left[a - b + \frac{1-\alpha}{2+\alpha} a^3 \left(\frac{1}{a^2} - \frac{1}{b^2}\right)\right] \cos\vartheta}{1 + 2\left(\frac{1-\beta}{2+\beta}\right)\left(\frac{1-\alpha}{2+\alpha}\right)\left(\frac{a}{b}\right)^3} \tag{15}$$

where $\alpha = \sigma_1/\sigma_2$ and $\beta = \sigma_2/\sigma_3$. Eq. 15 describes the dependence of V_M, which is superimposed on the intrinsic membrane potential, on the internal, external, and membrane conductivities and on the external electric field strength E_0.

Since in general $\sigma_1 \simeq \sigma_3 \gg \sigma_2$ for the cells considered in this paper (e.g., $\sigma_1 = 0.005$, $\sigma_2 = 1 \cdot 10^{-7}$ and $\sigma_3 = 0.01$ mho·cm^{-1} for human red blood cells [42]), it can be easily shown that Eq. 15 becomes

$$V_M = 1.5 \cdot b \cdot E_0 \cos\vartheta. \tag{16}$$

The solution of the Laplace equation in ellipsoidal coordinates (ξ_1, ξ_2, ξ_3) is more cumbersome. Here we present only the result which is obtained using the approximations described above:

$$V_M = f_i a_i E_0. \tag{17}$$

Here f_i is the shape factor and is expressed by the following equation:

$$f_i = 2\left[2 - a_1 a_2 a_3 \int_0^\infty \frac{ds}{(s + a_i^2)(\sum_{n=1}^{3}[s + a_n^2])^{1/2}}\right]^{-1} \tag{18}$$

where a_n denote the semi-axis and a_i the semi-axis parallel to the external electric field.

We are gratefully indebted to Dr. Coster (Sydney) for carefully reading and discussing the manuscript.

The authors should also like to thank H. J. Buers, H. Kock, and W. Petrick for their expert technical assistance.

This work was supported by a grant from the Deutsche Forschungsgemeinschaft, Bonn-Bad Godesberg, Sonderforschungsbereich 160.

Received for publication 28 May 1974.

REFERENCES

1. KUBITSCHEK, H. E. 1969. *In* Methods in Microbiology. J. R. Norris and D. W. Ribbons, editors. Academic Press, Inc., New York. **1**:593.
2. THOM, R., A. HAMPE, and G. SAUERBREY. 1969. *Z. Gesamte Exp. Med.* **151**:331.

3. GROVER, N. B., J. NAAMAN, S. BEN-SASSON, and F. DOLJANSKI. 1969. *Biophys. J.* **9**:1398.
4. GROVER, N. B., J. NAAMAN, S. BEN-SASSON, F. DOLJANSKI, and E. NADAV. 1969. *Biophys. J.* **9**:1415.
5. GROVER, N. B., J. NAAMAN, S. BEN-SASSON, and F. DOLJANSKI. 1972. *Biophys. J.* **12**:1099.
6. ZIMMERMANN, U., J. SCHULZ, and G. PILWAT. 1973. *Biophys. J.* **13**:1005.
7. ZIMMERMANN, U., and G. PILWAT. 1973. *In* Proceedings of the 9th International Congress of Biochemistry, Stockholm, 1–7 July 1973. 260.
8. ZIMMERMANN, U., G. PILWAT, and F. RIEMANN. 1974. *In* Membrane Transport of Plants. U. Zimmerman and J. Dainty, editors. Springer-Verlag, Berlin. In press.
9. THOM, R. 1972. AEG-Telefunken Publication No. N1/EP/V.
10. ZIMMERMANN, U., G. PILWAT, and F. RIEMANN. 1974. *Z. Naturforsch.* **29c**:304.
11. COSTER, H. G. L. 1965. *Biophys. J.* **5**:669.
12. COSTER, H. G. L., E. P. GEORGE, and R. SIMONS. 1969. *Biophys. J.* **9**:666.
13. COSTER, H. G. L. 1973. *Biophys. J.* **13**:1119.
14. BODEMANN, H., and H. PASSOW. 1972. *J. Membr. Biol.* **8**:1.
15. ZIMMERMANN, U., G. PILWAT, and T. GÜNTHER. 1973. *Biochim. Biophys. Acta.* **311**:442.
16. NEUMANN, E., and K. ROSENHECK. 1972. *J. Membr. Biol.* **10**:279.
17. ALLAN, R. S., and S. G. MASON. 1962. *Proc. R. Soc. Lond. Ser. A. Math. Phys. Sci.* **267**:45.
18. CROWLEY, J. M. 1973. *Biophys. J.* **13**:711.
19. SCHWARZ, G. 1962. *J. Phys. Chem.* **66**:2636.
20. WHITE, S. H., and T. E. THOMPSON. 1973. *Biochim. Biophys. Acta.* **323**:7.
21. RAND, R. P. 1964. *Biophys. J.* **4**:303.
22. KATCHALSKY, A., O. KEDEM, C. KLIBANSKY, and A. DE VRIES. 1960. *In* Flow Properties of Blood and other Biological Systems. A. L. Copley and G. Stainsby, editors. Pergamon Press, New York. 155.
23. HOCHMUTH, R. M., N. MOHANDAS, and P. L. BLACKSHEAR, JR. 1973. *Biophys. J.* **13**:747.
24. COLE, K. S. 1968. Membranes, ions and impulses. *In* Biophysics Series, Vol. 1. University of California Press, Berkeley, Calif.
25. RAND, R. P., and A. C. BURTON. 1964. *Biophys. J.* **4**:115.
26. SALE, A. J. H., and W. A. HAMILTON. 1967. *Biochim. Biophys. Acta.* **148**:781.
27. HAMILTON, W. A., and A. J. H. SALE. 1967. *Biochim. Biophys. Acta.* **148**:789.
28. KUBITSCHEK, H. E. 1968. *Biophys. J.* **8**:792.
29. OVERATH, P., H. U. SCHAIRER, F. F. HILL, and I. LAMNEK-HIRSCH. 1972. *In* The Dynamic Structure of Cell Membranes, 22nd Mosbacher Colloquium. D. F. Hölzl-Wallach and H. Fischer, editors. Springer-Verlag, Berlin. 149.
30. WHITE, S. H. *Biophys. J.* 1974. **14**:155.
31. JACKSON, J. D. 1962. Classical Electrodynamics. J. Wiley & Sons, Inc., New York.
32. EDER, G. 1967. Elektrodynamik, BI-Hochschultaschenbuch Nr. 233/233a. Bibliographisches Institut, Mannheim, West Germany.
33. STRATTON, J. A. 1941. Electromagnetic Theory. McGraw-Hill, New York.
34. FRICKE, H. 1924. *Phys. Rev.* **24**:575.
35. FRICKE, H. 1931. *Physics.* **1**:106.
36. FRICKE, H. 1953. *J. Appl. Phys.* **24**:644.
37. VELICK, S., and M. GORIN. 1940. *J. Gen. Physiol.* **23**:753.
38. MORSE, P. M., and H. FESHBACH. 1953. Methods of theoretical physics, parts I and II. *In* International Series in Pure and Applied Physics. McGraw-Hill, New York.
39. BERNHARDT, J., and H. PAULY. 1973. *Biophysik.* **10**:89.
40. TURNBULL, R. J. 1973. *J. Membr. Biol.* **14**:193.
41. NEUMANN, E., and K. ROSENHECK. 1973. *J. Membr. Biol.* **14**:194.
42. JOHNSON, S. L., and J. W. WOODBURY. 1964. *J. Gen. Physiol.* **47**:827.